International Journal of Nanomedicine

Dovepress
open access to scientific and medical research

Open Access Full Text Article

ORIGINAL RESEARCH

Hyaluronic Acid-Modified Micelles of Azithromycin and Quercetin Against Infections Caused by Methicillin-Resistant *Staphylococcus Aureus*

Zixu Zhang[1,2], Muhan Chen[1,2], Jiahua Wang[1,2], Mo Liu[1,2], Ruibo Guo[1,2], Lu Zhang[1,2], Liang Kong[1,2], Yang Liu[1,2], Yang Yu[1–3], Xuetao Li[1,2]

[1]School of Pharmacy, Liaoning University of Traditional Chinese Medicine, Dalian, 116600, People's Republic of China; [2]Shenyang Key Laboratory of Chinese Medicine targeted Delivery Key laboratory, Liaoning University of Traditional Chinese Medicine, Shenyang, 110847, People's Republic of China; [3]Key Laboratory of Ministry of Education for TCM Viscera-State Theory and Applications, Liaoning University of Traditional Chinese Medicine, Shenyang, 110032, People's Republic of China

Correspondence: Xuetao Li; Yang Yu, School of Pharmacy, Liaoning University of Traditional Chinese Medicine, Dalian, 116600, People's Republic of China, Tel +86411 8589 0170, Fax +86411 8589 0128, Email lixuetao1979@163.com; yuqn0702@163.com

Introduction: Resistance of intracellular pathogens is a challenge in microbial therapy. Methicillin-resistant *Staphylococcus aureus* (MRSA), which is able to persist inside the cells of infected tissues, is protected from attack by the immune system and many antimicrobial agents. To overcome these limitations, nano-delivery systems can be used for targeted therapy of intracellular MRSA.

Methods: Hyaluronic acid-modified azithromycin/quercetin micelles (HA-AZI/Qe-M) were synthesized by thin film hydration. The micelles were characterized by transmission electron microscopy (TEM), dynamic light scattering (DLS) and Fourier transform infrared spectroscopy (FTIR), and the drug loading (DL) and encapsulation efficiency (EE) were detected by high performance liquid chromatography (HPLC). The uptake ability of RAW264.7 cells was investigated, and its distribution in mice was evaluated by in vivo imaging. The inhibitory effect of the micelles against MRSA in vitro and its ability to eliminate intracellular bacteria were evaluated. Bacterial muscle-infected mice were constructed to evaluate the therapeutic effect of the micelles on bacterial infections in vivo and the biocompatibility of the micelles was investigated.

Results: HA-AZI/Qe-M had suitable physical and chemical properties and characterization. In vitro *a*ntibacterial experiments showed that HA-AZI/Qe-M could effectively inhibit the growth of MRSA, inhibit and eliminate the biofilm formed by MRSA, and have an excellent therapeutic effect on intracellular bacterial infection. The results of RAW264.7 cells uptake and in vivo imaging showed that HA-AZI/Qe-M could increase the cellular uptake, target the infection site, and prolong the treatment time. The results of in vivo antibacterial infection experiments showed that HA-AZI/Qe-M was able to ameliorate the extent of thigh muscle infections in mice and reduce the expression of inflammatory factors.

Conclusion: HA-AZI/Qe-M is a novel and effective nano-drug delivery system that can target intracellular bacterial infection, and it is expected to be safely used for the treatment of MRSA infection.

Keywords: MRSA, hyaluronic acid, antibiotics, micelles, azithromycin, quercetin

Introduction

Infectious diseases caused by pathogenic microorganisms pose a great threat to human health.[1] Scientific reports have proved that methicillin-resistant *Staphylococcus aureus* (MRSA) is one of the main causes of hospital-acquired infections, often causing muscle, skin, soft tissue and blood infections.[2,3] In addition, MRSA is a pathogen that can enter host cells, allowing intracellular bacteria to escape the host immune system attack, and host cells also provide shelter for intracellular bacteria to avoid drug attack.[4,5] More importantly, intracellular bacteria can also spread to different tissues from the site of infection in the host cells, causing meningitis, osteomyelitis, pulmonary infection, endocarditis and other diseases.[6–8] This kind of intracellular bacterial infection poses a great challenge to clinical treatment. Antibiotics are the first-line drugs for the treatment of bacterial infections, which have the characteristics of high antibacterial efficiency, wide range and low

Received: 2 July 2024
Accepted: 7 September 2024
Published: 16 September 2024

cost.[9,10] However, antibiotics are difficult to accurately target the site of infection, cause toxic side effects on tissues and organs, and even cause multi-drug resistance of bacteria due to excessive use of time or drug concentration.[11,12] In recent years, natural plant products have played a crucial role in drug development, and their secondary metabolic products have potential antibacterial activities, such as flavonoids, terpenoids, alkaloids, and phenols.[13,14] Bacteria have little resistance to natural plant products, so they are widely used in the study of antibacterial activity.[15,16]

Azithromycin (AZI, $C_{38}H_{72}N_2O_{12}$) is a macrolide antibiotic that has antibacterial activity against both Gram-positive and Gram-negative bacteria, and can be used in clinical practice to treat a variety of diseases such as respiratory infections, intestinal infections, and sexually transmitted infections.[17,18] Quercetin (Qe, $C_{15}H_{10}O_7$) is the most bioactive polyhydroxyl flavonoid among flavonoids and has been shown to be very effective against bacterial infections and inflammatory diseases.[19–21] Qe exerts its antibacterial effect against MRSA by inhibiting nucleic acid synthesis, destroying the bacterial membrane integrity, inhibiting biofilm formation and inhibiting the expression of virulence factors.[22,23] Due to bacterial resistance to antibiotics, poor water solubility, low dissolution rate, and low bioavailability of AZI and Qe have limited their application in clinical practice.[24] Therefore, in order to effectively cure bacterial infectious diseases, there is an urgent need to achieve the targeted delivery of antibacterial drugs to the lesion site to avoid drug damage to tissues and organs, so as to improve the therapeutic effect.

Nanotechnology has recently developed rapidly in the field of medicine, which has made breakthroughs in the treatment of bacterial infections and achieved excellent results. Currently, nanoparticles,[25,26] liposomes,[27,28] and micelles[29–31] with antibacterial effects, have been developed. Among these systems, micelle is a compelling nano-drug delivery system that can not only encapsulate hydrophobic drugs but also increase blood circulation time, thereby improving therapeutic efficiency.[32,33] Micelle has its unique properties, including small particle size, high stability, good biocompatibility, strong targeting, and adjustable surface modification.[34,35] Encapsulation of antibacterial drugs into micelles can effectively improve the permeability of the drug to the cell membrane and increase the uptake of the drug by cells.[36,37] Hyaluronic acid (HA, $(C_{14}H_{21}NO_{11})_n$) is a naturally occurring acidic mucopolysaccharide composed of D-glucuronic acid and N-acetylglucosamine linked by β −1, 4 - and β - 1, 3 - glycosidic bonds, and the molecular weight of HA ranges from 1 to 10000 kDa.[38] HA is widely distributed in the extracellular matrix of human connective tissues and has multiple physiological functions such as maintaining cellular structure and providing energy sources.[39] Hyaluronic acid has recently been widely used in biomedical applications due to its good biochemical properties such as biocompatibility, non-immunogenicity, and hydrophilicity.[40,41] CD44 is a transmembrane adhesion molecule, and its main function is to bind and internalize HA.[42] The specific binding of hyaluronic acid to CD44 into the body can lead to cytoskeletal reorganization, activate macrophages, and increase the ability of macrophages to phagocytize drug.[43] When the body is attacked by pathogens, the inflammatory response occurs, and the transmembrane glycoprotein CD44 is highly expressed on macrophages in the inflammatory site.[44]

In this study, we prepared a multifunctional micellar, hyaluronic acid-modified azithromycin and quercetin micelles (HA-AZI/Qe-M), targeting macrophages infected by bacteria, treating bacterial infections and the schematic is shown in Figure 1.

Materials and Methods

Materials and Reagents

AZI, lipopolysaccharide (LPS), D-a-Tocopherol polyethylene glycol 1000 succinate ($TPGS_{1000}$), Hoechst 33258 dye and gentamicin were supplied by Meilun Co., LTD. (Dalian, China). Soluplus was supplied by Basf New Materials Co., LTD. (Shanghai, China). Qe was purchased from Pufeide Biotechnology Co., LTD. (Chengdu, China). Polyethylene glycol-distearyl phosphatidylethanolamine (DSPE-PEG_{2000}), DSPE-PEG_{2000}-HA were purchased from Ruixi Biotechnology Co., LTD (Xi 'an, China). 1,1-dioctadecyl-3,3,3,3-tetramethylindotricarbocyanine iodide (DiR) was supplied by Keygen Biotechnology Development Co., Ltd. (Nanjing, China). Coumarin was obtained from Sigma-Aldrich Trading Company Co., Ltd. (Shanghai, China). *Staphylococcus aureus* (ATCC 29213) was purchased from Xin Yu Biotechnology Co., Ltd. (Shanghai, China). SYTO-9/PI kit was purchased from Fushen Biotech Co., Ltd. (Shanghai, China). LB Broth, LB agar, ELISA kits were supplied by Solarbio Co., LTD. (Beijing, China). All other reagents used were of analytical grade.

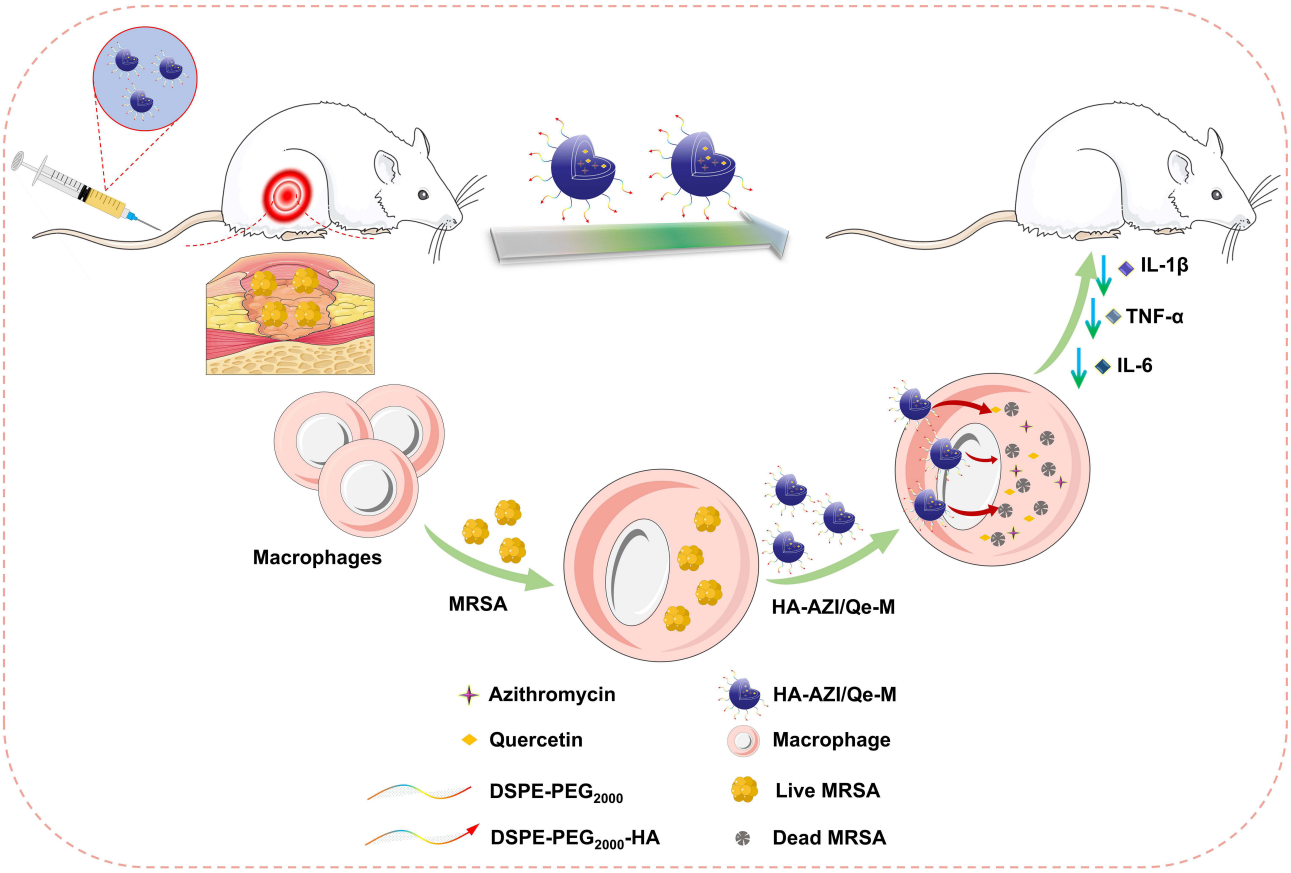

Figure 1 Schematic diagram of HA-AZI/Qe-M for the treatment of MRSA infection.

Mice and Cells

8 weeks BALB/c female mice (18–22 g) were purchased from Liaoning Changsheng Biotechnology Co., LTD. (Benxi, China). Mice were maintained in the Laboratory Animal Center of Liaoning University of Traditional Chinese Medicine at a constant temperature of 25 °C and 60% humidity, and cultured by exposure to sunlight for 12 h per day. All procedures with animals were approved by the Animal Research Ethics Committee of Liaoning University of Traditional Chinese Medicine (210,000420230202) and performed in accordance with the guidelines set forth in the Guide for the Care and Use of Laboratory Animals published by the National Institutes of Health (Eighth Edition).

Murine monocyte-macrophage leukemia cells (RAW264.7, serial: SCSP-5036, CSTR: 19375.09.3101MOUSCSP5036) cells were obtained from Institute of Basic Medical Sciences, Chinese Academy of Medical Sciences (Beijing, China). Cells were cultured in DMEM medium supplemented with 10% fetal bovine serum (FBS) and 1% penicillin-streptomycin (100 U/mL penicillin and 100 μg/mL streptomycin) at 37 °C in an air humidified atmosphere with 5% CO_2; these reagents were purchased from GIBCO (Billings, MT, USA).

Preparation of Micelles

Using a thin-film dispersion method, we prepared HA-AZI/Qe-M.[45] Briefly, 80 mg of Soluplus, 20 mg of TPGS, 2 mg of DSPE-PEG_{2000}, 2 mg of DSPE-PEG_{2000}-HA, 1 mg of AZI and 2.5 mg of Qe, were placed in a round-bottom flask and dissolved with methanol. The round-bottom flask containing the above samples was then rotated in a rotary evaporator at 40 °C until the methanol was completely evaporated to form a thin film. The film was then hydrated with 5 mL phosphate buffered saline (PBS, pH 7.4, 0.01M) and the film was sonicated into PBS in a water bath to obtain hydrated micelles (bath sonication conditions: operating frequency 40KHz, ultrasonic power 150W). The sample obtained from hydration was penetrated twice through a 0.22 μm polycarbonate membrane to obtain HA-AZI/Qe-M. Blank micelles (Blank-M),

azithromycin micelles (AZI-M), azithromycin and quercetin micelles (AZI/Qe-M), coumarin micelles (Coumarin-M), and DiR micelles (DiR-M) were also prepared according to the same procedure.

Characterization of Micelles

The shape of micelles was observed by transmission electron microscopy (TEM, JEM-1200EX; JEOL, Tokyo, Japan). Particle size, zeta potential and polydispersity index (PDI) were determined using a dynamic light scattering instrument (DLS, Zetasizer Nano ZS90, Malvern, UK). The molecular functional groups of micelles were investigated by Fourier transform infrared spectroscopy (FTIR-850, Tianjin, China). The unencapsulated drug was removed on a Sephadex G-50 column, and AZI and Qe contents were determined by high-performance liquid chromatography (HPLC) equipped with an ultraviolet detector. The encapsulation efficiency (EE) was calculated using the formula: $EE\% = (W_1/W_2) \times 100\%$, where W_1 and W_2 represented the content of drug after and before elution. The drug loading (DL) was calculated using the formula: $DL\% = (W_3/W_4)$, W_3 and W_4 represent the amount of drug within the micelles and the total weight of the drug-loaded micelles.

Synergy Determination with SynergyFinder

The strain of MRSA used in this study is ATCC 29213, with a diameter of 0.5–1μm. It has the characteristics of rapid growth and is collected from human wound sites. MRSA was inoculated into 96-well plates at 2×10^7 CFU/well. AZI and Qe were diluted at a certain concentration (AZI concentration: 20, 10, 5, 2.5, 1.25, and 0.625 μg/mL, Qe concentration: 50, 25, 12.5, 6.25, 3.125, and 1.5625 μg/mL) and mixed with MRSA for 8 h. The absorbance of bacteria at 600nm represents the density of the bacteria, OD_{600} between 0.6 and 0.8 represents that the bacteria are in the logarithmic growth phase, and more than 1.0 represents that the bacteria are saturated. Therefore, OD_{600} values per well were measured hourly using a microplate reader (Synergy H1, Biotek, USA), and the synergy scores of the drugs were calculated using the online *SynergyFinder* software to calculate the zero interaction potentials (ZIP) of the two drugs.[46]

Cytotoxic Effects on RAW264.7 Cells

The cytotoxicity of drugs on RAW264.7 cells was evaluated using the sulforhodamine B (SRB) assay.[47] After the RAW264.7 cells were attached to the wall, the cells were observed under the electron microscope, and the confluence rate reached 70–80%. At this time, the cells were in log phase. RAW264.7 cells in logarithmic growth phase were inoculated in 96-well plates at a density of 1.5×10^4 cells/well, and incubated in an incubator at 37 °C and 5% CO_2 for 24 h. The administration groups were given AZI, AZI-M, AZI/Qe-M, HA-AZI/Qe-M and Blank-M treatments, respectively (AZI concentration range: 0–20 μg/mL; Qe concentration range:0–50μg/mL). After the cells were treated with drugs for 48 h, the culture medium was discarded and 200 μL of 10% trichloroacetic acid was added to each well. Cells were fixed at 4 °C for 1 h, washed five times with distilled water, and then stained with 0.4% SRB for 20 min, and finally washed with 1% acetic acid solution to remove unbound SRB dye. The absorbance was measured at 540 nm after shaking with 200 μL (10 mmol/L) of Tris buffer per well for 30 min. Cell viability was calculated as follows: $\text{viability}\ (\%) = (A_1/A_0) \times 100\%$, where A_1 and A_0 represent the absorbance at 540 nm of treated cells and blank control cells, respectively.

Cellular Uptake Assay

RAW264.7 cells were inoculated into 6-well plates (3×10^5 cells/well) and after cell adherence, LPS (100 ng/mL) was added to each well for induction overnight.[48] Flow cytometry was used to detect the uptake of different micelles by RAW264.7 cells. Blank-M, Coumarin-M, and HA-modified coumarin micelles (HA-Coumarin-M) were added to the above 6-well plates (final concentration of coumarin was 3 μM). After incubating at 37 °C for 2 h, the cells were resuspended in 500 μL of PBS. The mean fluorescence intensity of coumarin was determined by flow cytometry (BD Biosciences, NJ, USA).

Confocal laser scanning microscope (CLSM) was used to observe the uptake of different formulated micelles by RAW264.7 cells. RAW264.7 cells were inoculated into confocal dishes (3×10^4 cells/dish), then cells were incubated with micelles of different formulations as described above, and after 4 h of incubation, cells were washed three times

with PBS and then fixed with p-formaldehyde (4%) at room temperature for 10 min. The above samples stained with Hoechst 33258 dye for 15 min in the dark, and subsequently observed under CLSM (HOOKE S3000, HOOKE Instruments Ltd, China).

Hemolysis Rate Determination

2% Red blood cells (RBC) suspension was prepared with fresh mouse blood,[49,50] 1.5 mL RBC suspension was added to each group, and then 0.5 mL HA-AZI/Qe-M (0.125 mg/mL, 0.25 mg/mL, 0.5 mg/mL, 1 mg/mL, 2 mg/mL), normal saline and water were added according to the group. Above samples were incubated in incubators at 37 °C for 5 h, then centrifuged, and the supernatant was aspirated (saline was used as a negative control and water as a positive control). The supernatant was transferred to a 96-well plate and the absorbance at 540 nm was measured using a microplate reader (HBS-1096A, DeTie, Nanjing, China). Hemolysis rate (HR%) = $(A_{sample} - A_{negative})/(A_{positive} - A_{negative}) \times 100\%$.

Inhibition Zone Determination

First, 100 μL of MRSA (1×10^9 CFU/mL) solution was applied on LB solid medium and spread evenly. Then drug-sensitive paper sheets with 30 μL of AZI, AZI-M, AZI/Qe-M, HA-AZI/Qe-M and Blank-M (AZI concentration: 200 μg/mL; Qe concentration: 500 μg/mL) drops were placed on the medium, respectively. After the aforementioned steps, all petri dishes were incubated at 37 °C for 24 h. The diameter of inhibition zone was recorded for each group.

Determination of Minimum Inhibitory Concentration (MIC)

180 μL of MRSA (1×10^9 CFU/mL) was first inoculated into 96-well plates, and 20 μL AZI, AZI-M, AZI/Qe-M, HA-AZI/Qe-M, and Blank-M (AZI concentration range: 0.3125–20 μg/mL; Qe concentration range: 0.7813–50 μg/mL) were mixed with the MRSA bacterial solution. The positive control was 180 μL of bacterial solution and 20 μL of sterile water, and the negative control consisted of 180 μL of LB broth medium and 20 μL of sterile water. After incubation at 37 °C for 24 h, the above samples were incubated in a microplate reader (Synergy H1, Biotek, USA). The MIC of the drug against MRSA was determined as the lowest concentration in which no bacterial growth was observed (OD_{600} did not increase). The MIC mentioned in the subsequent studies were those of AZI against MRSA.

Growth Experiments

MRSA was inoculated in 96-well plates (2×10^8 CFU/well) and AZI, AZI-M, AZI/Qe-M, HA-AZI/Qe-M and Blank-M (control) were all added at 1/2MIC. The above samples were placed in the incubator at 37 °C for 24 h, during which the OD_{600} value of each well was measured every 1 h with an microplate reader (Synergy H1, Biotek, USA), and the growth curves of each group of MRSA in 24 h were plotted according to the value of OD_{600}.

Live and Dead Staining of Bacteria

MRSA were treated with different groups of drugs (MIC) and incubated in an incubator for 3 h. Above samples were centrifuged and stained by adding propidium iodide (PI) and SYTO 9 Green Fluorescent Nucleic Acid Stain (SYTO-9) to avoid light for 30 min. At the end of the staining, the bacteria were washed with PBS for 3 times, and 10 μL of bacterial fluids were taken on slides, and then covered with a coverslip and observed by CLSM (Mica, Leica, GER).

Anti-intracellular Bacterial Infection Experiment

RAW264.7 cells were inoculated in 24-well plates and cultured for 24 h until the cells fused into a monolayer. MRSA was then inoculated into RAW264.7 cells at a ratio of bacteria: cells= 100:1. After incubating the cells and bacteria for 2 h at 37 °C, DMEM medium containing 100 μg/mL gentamicin was added and incubated for 1 h to kill the extracellular free bacteria. After three washes with PBS, the above samples were treated with different groups of drugs (MIC) for 12 h. The medium was then rinsed with PBS and 100 μL of 0.5% Triton X-100 to lysed cells for 8 min, and immediately added 100 μL PBS to blow up. The cell lysates were diluted in PBS gradient, and the diluted cell lysates were then spread on plates and cultured until obvious colonies were formed, and the number of colonies was counted. The intracellular bacterial load is represented as CFU/well.

Biofilm Inhibition Test

The inhibitory effect of drugs on biofilm formation was first evaluated by crystal violet staining.[51] MRSA was inoculated into 96-well plates (2×10^8 CFU/Well), and different groups of drug treatments (MIC) were added and incubated at 37 °C for 24 h. The liquid was discarded from the 96-well plate, then washed three times with PBS and the plate was fixed with methanol for 15 min and the excess methanol was aspirated. After being allowed to dry naturally at room temperature, 200 μL of crystal violet solution at a concentration of 0.4% was added and incubated for 15 min at room temperature, followed by aspiration of excess dye and 3 washes with PBS. After again leaving to dry naturally at room temperature, 200 μL of 33% glacial acetic acid dissolution fuel was added to each well and absorbance was measured at 590 nm. Similarly, MRSA was inoculated in 24-well plates and treated as described above, and biofilm crystal violet staining was observed under a fluorescence microscope (Nikon Eclipse E800, Nikon, Tokyo).

Fluorescence confocal dishes were inoculated with MRSA, incubated at 37 °C for 24 h, then treated with different groups of drugs (MIC), and incubated for another 8h. After washing with PBS for 3 times, SYTO-9/PI dye was added and incubated at 37 °C for 30 min in dark condition, followed by aspirating the excess dye, washing with PBS for 3 times, and drying naturally at room temperature, and then photographed with CLSM (Mica, Leica, GER) to observe the fluorescence.

Establishment and Treatment of Mouse Muscle Bacterial Infection Model

Thirty six 8-week-old female mice were randomly divided into six groups: control, model, AZI, AZI-M, AZI/Qe-M group, and HA-AZI/Qe-M groups. Mice were injected intramuscularly with 100 μL of MRSA (1×10^8 CFU/mL). 24 h after bacterial injection, mice were injected with 200 μL of the corresponding drug in the tail vein every 48 h and administered three times consecutively.

After 7 days of treatment, mice were euthanized. Hematoxylin and eosin (HE) staining and Masson staining were performed to observe the integrity of muscle structure, muscle tissue necrosis and inflammatory cell infiltration. Changes in the infectious injury of mouse thigh muscles during the treatment period were recorded. Blood was collected from the eyeballs of the mice, and serum was obtained by freezing and centrifugation. The serum levels of tumor necrosis factor-α (TNF-α), interleukin-6 (IL-6) and interleukin-1β (IL-1β) were detected by ELISA. Mouse muscle tissues were homogenized and plated, and the number of colonies on the coated plates was counted after incubation at 37 °C for 24 h.

In vivo Fluorescence Imaging

To evaluate the real-time distribution of HA-AZI/Qe-M in vivo, a non-invasive optical imaging system was used. DiR was encapsulated into micelles as a fluorescent probe. 100 μL of saline, DiR, DiR-M, and HA-DiR-M were injected via the tail vein (DiR concentration was 200 μg/kg, and free DiR was dissolved in 10% ethanol + 90% PBS). Mice were anesthetized with isoflurane, and fluorescent images of the mice were captured at 3, 6, 12, 24, 36, 48, 72, and 96 h using an in vivo fluorescence imaging system (CareStream, Health Inc., USA).

Biocompatibility

To evaluate the biocompatibility of the drug, we first recorded the changes in body weight of the mice during the treatment. After euthanasia of mice, heart, kidney, liver, spleen and lung were taken for histological analysis. Serum was also collected for blood chemistry studies, including the liver function indices of alanine aminotransferase (ALT) and aspartate aminotransferase (AST).

Statistical Analysis

Statistical analysis was performed using GraphPad Prism 8.0.2 software, and the data were expressed as the mean ± standard deviation (mean ± SD). Differences more than three groups were assessed by one-way analysis of variance (ANOVA) and Student's test for two groups. $P < 0.05$, the difference was significant and statistically significant.

Results

Characterization of Micelles

The chemical structural formulas of AZI, Qe, and HA are shown in Figure 2A–C. As shown in Figure 2D, we observed the shape of HA-AZI/Qe-M by TEM, which had a spheroidal shape with a uniform size and a particle size of about 130 nm. In the FTIR, as shown in Figure 2E, the stretching vibration of ether bond (C-O-C), carbonyl group (C=O) and hydroxyl group (O-H) in Qe was 1311 cm^{-1}, 1670 cm^{-1} and 3346 cm^{-1}, respectively. The stretching vibration of carbonyl group (C=O) in azithromycin was 1721 cm^{-1}, the stretching vibration of ether bond (C-O-C) was 1052 cm^{-1}, and the stretching vibration of hydroxyl group (O-H) was 3496 cm^{-1} and 3561 cm^{-1}. The stretching vibrations in the blank micelles (C-H) were 2921 cm^{-1} and 2837 cm^{-1}, and the carbonyl group (C=O) was 1730 cm^{-1}. The particle size distribution and PDI, as well as the zeta potential values of the four micelles were measured by dynamic light scattering. Figure 2F and G indicated the particle size distribution and zeta potential value plots of Blank-M, and the average particle size of Blank-M was 74.13 ± 1.25 nm, and the average zeta potential value was −2.17 ± 0.12 mV. Figure 2H and I show the particle size distribution and zeta potential value of HA-AZI/Qe-M. The average particle size of HA-AZI/Qe-M is 127.47 ± 3.64 nm, and the average zeta potential value is −2.63 ± 0.21 mV. Figure 2J–L and Table 1 show the average particle size, zeta potential values, and PDI values of the four groups of different micelles. The results showed that the average particle size of HA-AZI/Qe-M was about 124.47 ± 3.64 nm, the zeta potential was about −2.63 ± 0.21 mV, and the PDI was about 0.24 ± 0.03. Figure 2M shows that the EE of AZI/Qe-M is 89.55 ± 1.14%, and that of HA-AZI/Qe-M is 89.55 ± 2.57%. Figure 2N shows that the DL of AZI and Qe in AZI/Qe-M were 2.18 ± 0.16% and 2.47 ± 0.07%. The DL of AZI and Qe in HA-AZI/Qe-M were 2.59 ± 0.13% and 2.30 ± 0.15%.

Synergy Determination with SynergyFinder

To determine the favorable ratio of AZI and Qe, we calculated the drug ZIP synergy score using the online software *SynergyFinder*, and determined the ratio used for the two drugs based on synergy experiments. As shown in Figure 3A, ZIP synergy score of the two drugs was 7.005, indicating that AZI and Qe had a good synergistic effect on combined antibacterial activity (10 > ZIP synergy score > 0), the white rectangle is the maximum synergistic effect area. Combined with previous encapsulation efficiency experiments, we chose azithromycin concentration of 20 μg/mL and quercetin concentration of 50 μg/mL as the combination concentration for the following study.

RAW264.7 Cytotoxicity Assay

The cytotoxicity of the micelles was further determined according to the concentration ratio of the combination of the two drugs determined by the synergy experiment. The in vitro cytotoxicity of AZI, AZI-M, HA-AZI/Qe-M, and Blank-M at different concentrations on RAW264.7 cells was studied. As shown in Figure 3B, the cell survival rate was greater than 80% in each group within the range of drug concentrations administered.

RAW264.7 Cell Uptake

As shown in Figure 4A and B, the level of FL1-H in HA-Coumarin-M treated cells was greater than that in the Coumarin-M. Figure 4C and D show the fluorescence image and fluorescence quantification diagram of coumarin uptake in cells observed by CLSM. The results show that the fluorescence of coumarin in cells treated with HA-Coumarin-M is the strongest and the amount of fluorescence absorbed is the largest.

In vitro Antibacterial Experiments

MRSA (ATCC 29213) was used in this study. As shown in Figure 5A and B, the diameter of inhibition zone was 15.42 ± 0.61mm in AZI group, 15.48 ± 0.57mm in AZI-M group, 17.17 ± 0.41mm in AZI/Qe-M group, and 17.48 ± 0.32mm in HA-AZI/Qe-M group. (a: control, b: AZI group, c: AZI-M group, d: AZI/Qe-M group, e: HA-AZI/Qe-M group). Figure 5C shows the MIC of different groups of drugs against MRSA. The MIC of AZI and AZI-M for MRSA was 2.5 μg/mL, and the MIC of AZI/Qe-M and HA-AZI/Qe-M was 1.25 μg/mL. We then incubated MRSA with AZI, AZI-M, AZI/Qe-M, and HA-AZI/Qe-M and examined the OD_{600} values of MRSA detected at one-hour intervals over 24 h. As shown in Figure 5D, although the OD_{600} values of MRSA in AZI group and AZI-M group were significantly lower than

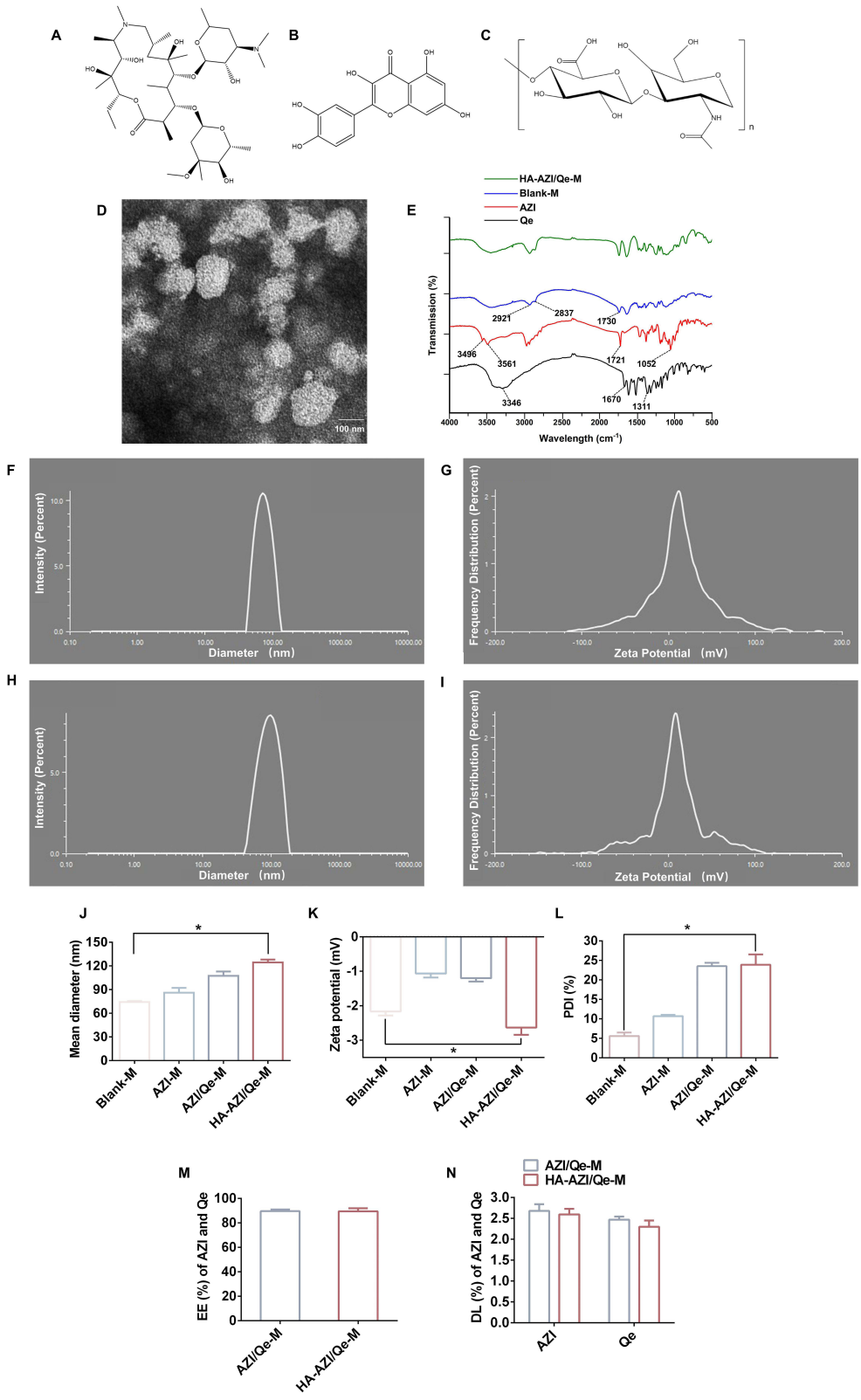

Figure 2 Characterization of HA-AZI/Qe-M. (**A**) Structural formula for AZI. (**B**) Structural formula for Qe. (**C**) Structural formula for HA. (**D**) Transmission electron microscopy images of HA-AZI/Qe-M. (**E**) FTIR spectra of Qe, AZI, and HA-AZI/Qe-M. (**F**) Particle size distribution of Blank-M. (**G**) Zeta potential distribution of Blank-M. (**H**) Particle size distribution of HA-AZI/Qe-M. (**I**) Zeta potential distribution of HA-AZI/Qe-M. (**J**) Particle size distribution of different micelles. (**K**) Zeta potential distribution of different micelles. (**L**) PDI distribution of zeta for different micelles. (**M**) EE of HA-AZI/Qe-M. (**N**) DL of HA-AZI/Qe-M. Scale bar: 100 nm. Data are presented as means ± SD (n = 3). *$P < 0.05$.

Table 1 Particle Size, PDI, and Zeta Potential of the Micelles (n=3).

Micelles	Particle Size (nm)	Polydispersity Index (PDI)	Zeta Potential (mV)
Blank-M	74.13 ± 1.25	0.056 ± 0.09	−2.17 ± 0.12
AZI-M	86.04 ± 6.12	0.107 ± 0.03	−1.07 ± 0.12
AZI/Qe-M	107.44 ± 5.50	0.24 ± 0.01	−1.2 ± 0.1
HA-AZI/Qe-M	124.47 ± 3.64	0.24 ± 0.03	−2.63 ± 0.21

those in control group, the antibacterial effect was not obvious, while the OD_{600} values of AZI/Qe-M and HA-AZI/Qe-M groups were lower, and the growth inhibition of MRSA was stronger.

To investigate the bactericidal effect of micelles on MRSA, we stained with the Live/Dead kit and observed bacterial survival and death with CLSM. Live bacteria appear green, and dead or dying bacteria appear red. As shown in Figure 5E, all the bacteria in the blank control group showed green fluorescence. Compared with the control group, the green fluorescence in the AZI and AZI-M groups was weakened, and some red fluorescence appeared, indicating that some bacteria were killed in the AZI and AZI-M groups, and the bactericidal effect was good. We observed that the green fluorescence of HA-AZI/Qe-M group was significantly weakened and a large number of red fluorescence appeared, indicating that HA-AZI/Qe-M killed most of the bacteria and had stronger bactericidal effect.

Intracellular Bacterial Experiments

With the increasing resistance of bacteria to antibiotics, intracellular bacterial infection caused by MRSA has become a difficult problem to solve. As shown in Figure 5F, compared with the control group, AZI can kill a certain amount of intracellular bacteria. AZI-M and AZI/Qe-M can kill most of the intracellular bacteria, but the antibacterial effect is far less than HA-AZI/Qe-M.

Inhibition of Biofilm Research

Biofilm generated by bacteria is one of the reasons why bacteria are resistant to antibiotics and have poor therapeutic effect. At the early stage of biofilm formation, we used crystal violet staining to evaluate the inhibitory effect of MRSA biofilm after different drug treatments. As shown in Figure 6A–C, the crystal violet staining results showed that HA-AZI/Qe-M effectively inhabited the biofilm formed by MRSA and it was superior to free AZI and AZI-M. We also stained the bacteria with Live/Dead kit and observed the disruption of the biofilm by the drugs with CLSM. As shown in Figure 6D, after the treatment of MRSA-formed biofilm by different drugs, the HA-AZI/Qe-M group showed strong red fluorescence, indicating that HA-AZI/Qe-M had a strong scavenging effect on biofilm.

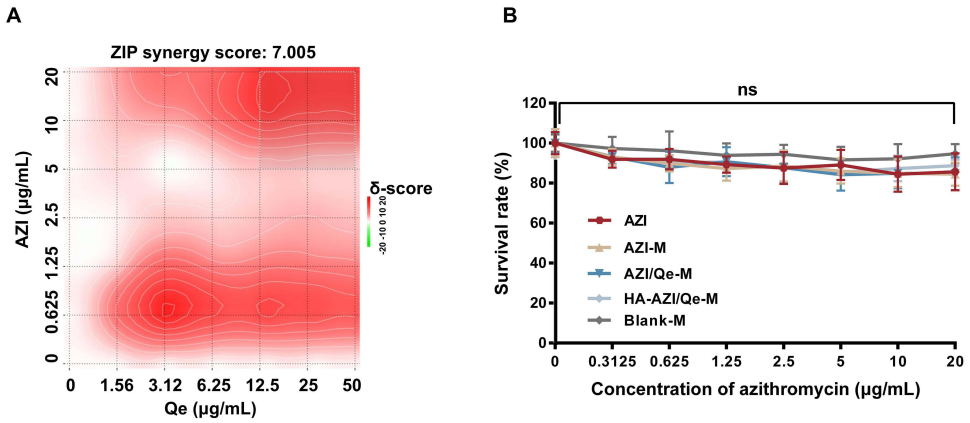

Figure 3 Synergy determination with SynergyFinder and RAW264.7 cytotoxicity assay. (**A**) Heatmaps of drug combination responses. ZIP Synergy scores were calculated using Synergyfinder software. Scores > 0 indicated synergism, and scores > 10 were considered strong synergistic (n = 4). (**B**) Survival rate of RAW264.7 cells after treatment with different groups of drugs at different concentrations of AZI (n = 5). Data are presented as means ± SD (n = 4 or 5). ns = no significance.

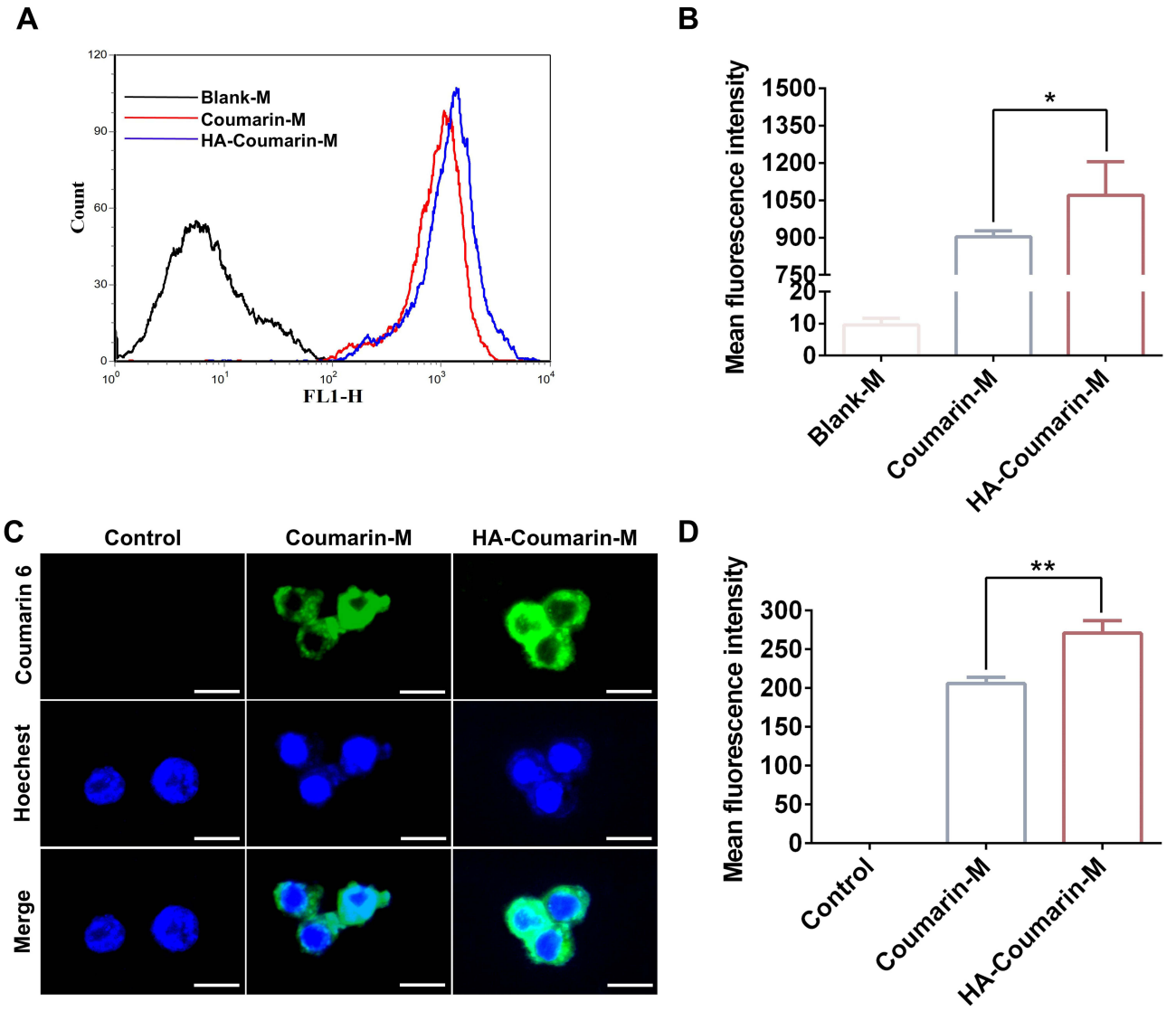

Figure 4 Uptake and distribution of RAW264.7 cells after incubation with micelles of different formulations. (**A**) RAW264.7 Uptake of cells. (**B**) Quantitative analysis of fluorescence intensity. (**C**) Confocal fluorescence images of RAW264.7 cells incubated in different formulations of micelles. (**D**) Average fluorescence intensity of RAW264.7 cells. Scale bar: 20 μm. Data are presented as means ± SD (n = 3). *$P < 0.05$, **$P < 0.01$.

In vivo Fluorescence Imaging in Mice

To demonstrate that HA-AZI/Qe-M can better target the MRSA infection site in vivo, we replaced the drug within the micelles with the fluorescent probe DiR (concentration of DiR: 10 μg/mL). Drug distribution in MRSA infected mice was evaluated by in vivo imaging at 3 h, 6 h, 12 h, 24 h, 48 h, 72 h, and 96 h after tail vein injection of free DiR and DIR-M and HA-DiR-M. As shown in Figure 7, after 96 h of administration, there was no fluorescence in the mice of the DiR group, while DiR-M and HA-DiR-M still had fluorescence in the mice, and the fluorescence intensity of HA-DiR-M was the strongest, which may be related to the effect of DSPE-PEG_{2000}-HA.

Anti-Bacterial Effect of HA-AZI/Qe-M in vivo

In this study, we further evaluated the anti-infective effect of HA-AZI/Qe-M on MRSA muscle-infected mice, and we divided the mice into control, model, AZI, AZI-M, AZI/Qe-M, and HA-AZI/Qe-M groups. In vivo anti-infective treatment was carried out as shown in Figure 8A. After intramuscular injection of MRSA for 24 h, the thighs of mice showed redness and swelling, and even slight ulceration, which indicated that the model was

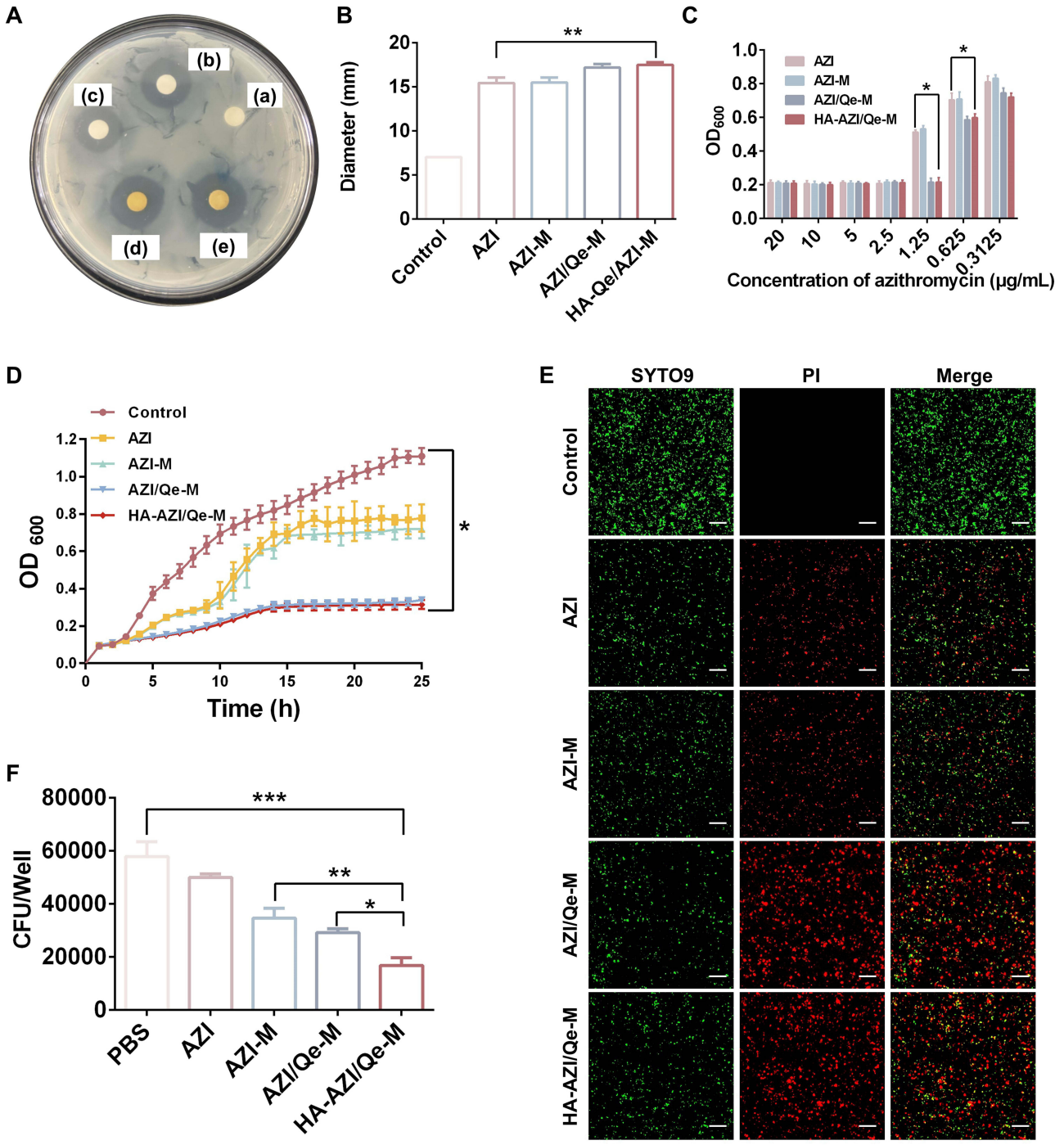

Figure 5 In vitro antibacterial effect of HA-AZI/Qe-M. (**A**) Circle of inhibition of different groups of drugs. (**a**) Blank-M; (**b**) AZI; (**c**) AZI-M; (**d**) AZI/Qe-M; (**e**) HA-AZI/Qe-M. (**B**) Histogram of the circle of inhibition of different groups of drugs. **(C)** Minimum inhibitory concentrations of different groups of drugs against MRSA. (**D**) Growth curves of MRSA within 24 h of different groups of drug treatments. (**E**) Confocal imaging of MRSA with death/live staining after treatment with different groups of drugs. (**F**) Bacterial counts in MRSA-infected RAW264.7 cells treated with different groups of drugs. Scale bar: 20 μm. Data are presented as mean ± SD (n =3). **P* < 0.05, ***P* < 0.01, ****P* < 0.001.

successful. After successful modeling of the mice, drugs were injected into the tail vein every 48 h for three times. As shown in Figure 8B, we photographed and recorded the changes of the infection site in each group of mice during the treatment period, and the infection site of the HA-AZI/Qe-M group had recovered to be comparable to that of the blank group at the end of the treatment, which was a significant control with the model group.

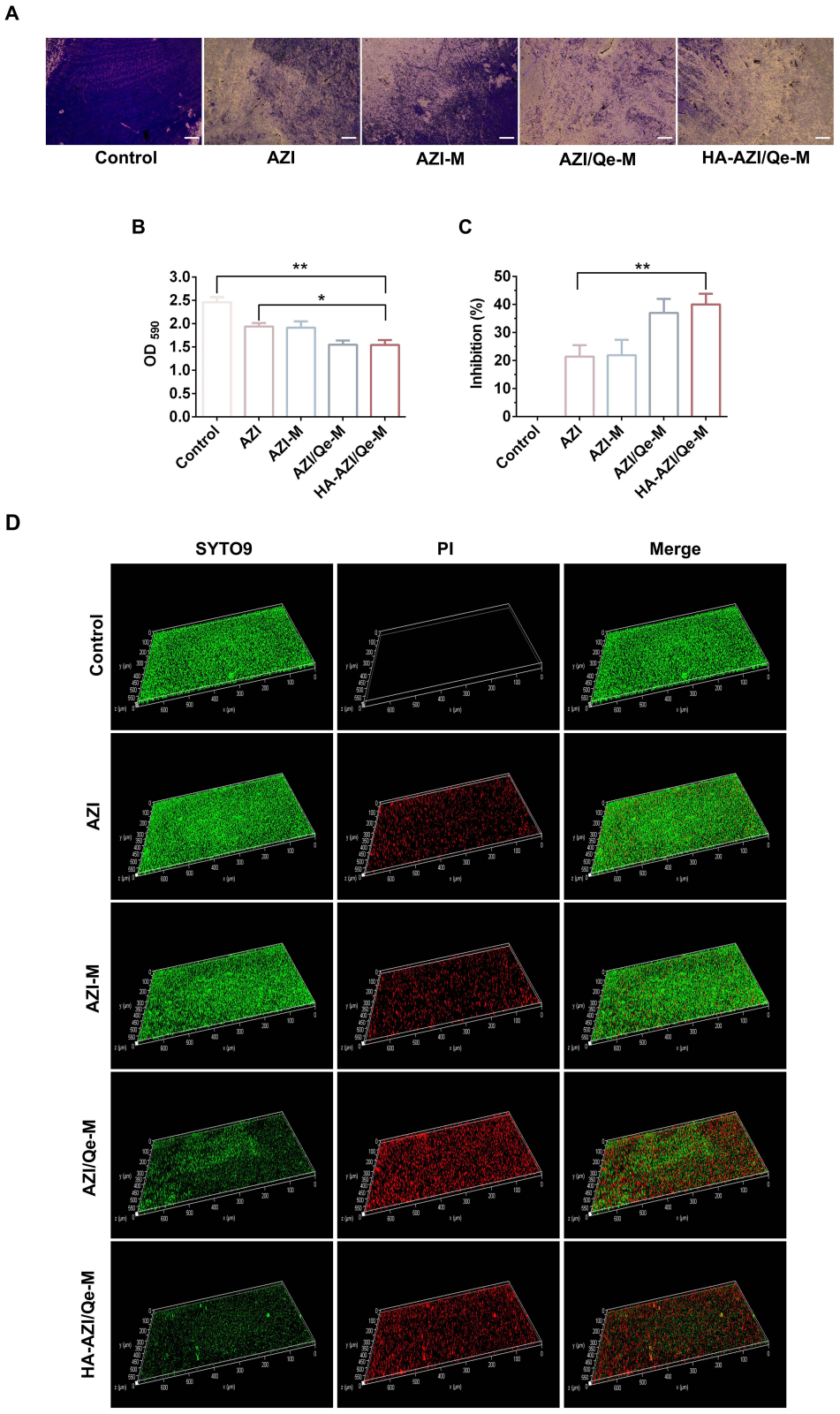

Figure 6 Inhibition of MRSA biofilms. (**A**) Crystal violet staining of biofilm (n = 8). (**B**) Absorbance of the biofilm at 590 nm (n = 8). (**C**) Biofilm inhibition rate of different groups (n = 8). (**D**) Confocal imaging of MRSA biofilms (n = 6). Scale bar: 100 μm. Data are presented as mean ± SD (n = 6 or 8). *P < 0.05, **P < 0.01.

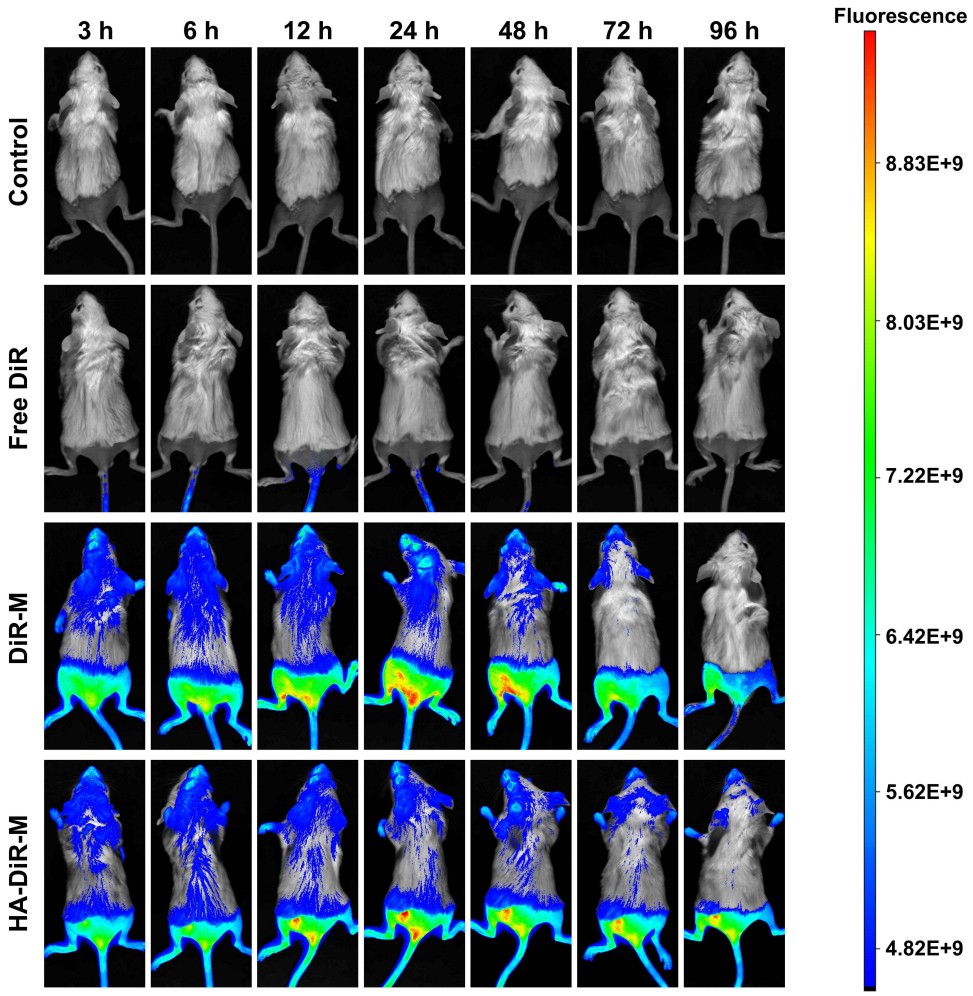

Figure 7 Real-time imaging observation in mice after intravenous administration (n = 3).

After the end of treatment, the muscle tissues of mice in each group were collected for HE staining and Masson staining to observe the integrity of muscle tissue structure and the inflammation, necrosis, and inflammatory cell infiltration and fibrosis. As shown in Figure 8C and D, the results showed that the improvement of muscle tissue in HA-AZI/Qe-M group was significantly better than that in AZI, AZI-M and AZI/Qe-M groups, and there was basically no damage to muscle tissue structure and no inflammatory cell infiltration. The muscle tissues of different groups of mice were homogenized and plated to count the number of colonies. As shown in Figure 8E and F, compared with the control group, the AZI group had a significant reduction in the number of bacteria in muscle homogenate, but the HA-AZI/Qe-M group had the lowest number of colonies.

Serum levels of IL-1β, IL-6 and TNF-α were measured by ELISA. As shown in Figure 8G, the levels of IL-1β, IL-6 and TNF-α in AZI, AZI-M and AZI/Qe-M groups were significantly increased compared with the blank group, while the levels of IL-1β, IL-6 and TNF-α in HA-AZI/Qe-M group returned to the same level as the control group.

Biocompatibility

To evaluate the blood compatibility of HA-AZI/Qe-M, we performed a hemolytic test. As shown in Figure 9A and B, we co-incubated 2% RBCs with different concentrations of HA-AZI/Qe-M, and the hemolysis of HA-AZI/Qe-M were all less than 5%.

In order to evaluate the biocompatibility of HA-AZI/Qe-M, we recorded the body weight changes of mice within seven days of drug administration. As shown in Figure 9C, the body weights of mice in the control group showed a certain increase, while the body weights of mice in the remaining four dosing groups showed a decreasing and then

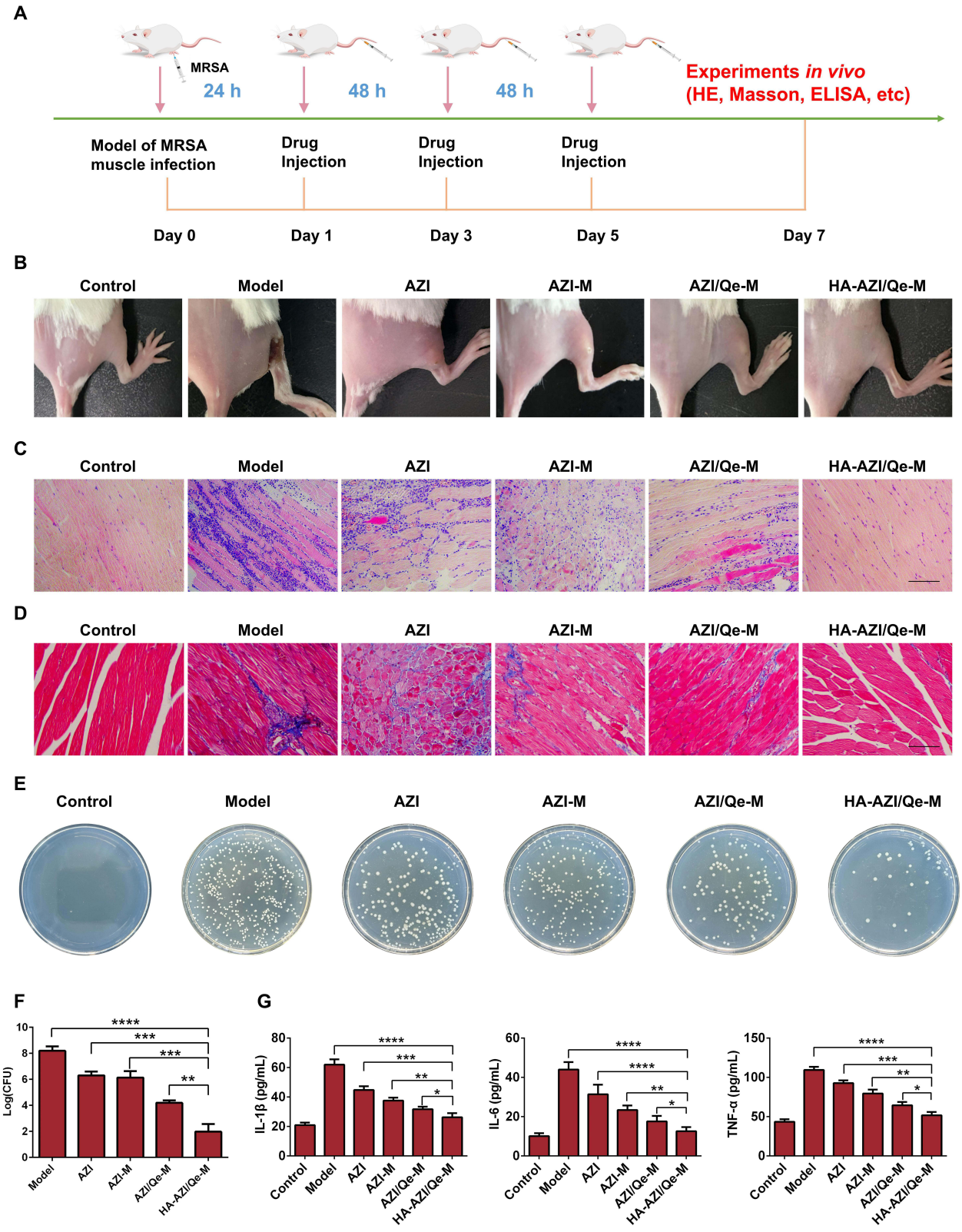

Figure 8 Anti-infection effect of HA-AZI/Qe-M in vivo. (**A**) Schematic diagram of in vivo anti-infection experimental design. (**B**) Representative photographs of infected thighs of mice seven days after treatment (n = 6). (**C**) HE staining of muscle tissue (n = 6). (**D**) Masson staining of muscle tissue (n = 6). (**E** and **F**) Bacterial counts in muscle homogenates (n = 3). (**G**) Levels of inflammatory factors (n = 3). Scale bar: 50 μm. Data are presented as mean ± SD (n = 3 or 6). **P* < 0.05,***P* < 0.01,****P* < 0.001,*****P* < 0.0001.

increasing trend. Figure 9D shows the AST and ALT of the treated mice, and the results show that the ALT and AST values of the treated group were not significantly different from control group, indicating that our preparation was not hepatotoxic to the mice.

To further evaluate the toxicity of the drug, we evaluated the pathological changes of five groups of organs (heart, liver, spleen, lung and kidney) by HE staining. As shown in Figure 9E, no fibrosis, necrosis, or histological abnormality were observed in the pathological sections of organs in each group. In summary, the results showed that HA-AZI/Qe-M did not cause significant damage to heart, liver, spleen, lungs and kidneys, and had a good biocompatibility.

Discussion

The physicochemical properties of micelles, such as particle size, zeta potential, PDI, encapsulation efficiency, and drug loading, are important for their pharmacokinetics and biodistribution. The surface of HA-AZI/Qe-M smooth and spherical in shape as seen by the TEM images. FTIR showed that in HA-AZI/Qe-M, the characteristic peaks of AZI and Qe disappeared, and only the characteristic peak of Blank-M was left, indicating that the drug may be encapsulated in micelles. The increased particle size of HA-AZI/Qe-M compared to Blank-M indicated that the drug was encapsulated by micelles, and the results were consistent with FTIR. The narrow PDI indicates that the micelles are uniformly distributed. Both HA and DSPE-PEG_{2000} were negatively charged,[52,53] so HA-AZI/Qe-M had the most negative charge among the four micelles. The negative charge on the micelle surface may help to reduce its nonspecific interactions in vitro and in vivo.[54]

Biomaterials should be non-toxic or low toxic and not affect normal cell function.[55] RAW264.7 cells, which have been widely used in terms of cytotoxicity and viability, were used as the model cells in this study.[56] On the basis of this administration concentration, we performed cytotoxicity experiments of different drugs on RAW264.7 cells for cell viability assay. Based on the results of synergy experiments, the survival rates of RAW264.7 cells treated with different drugs were investigated. As shown in the results, the concentration of AZI was increased from 0 to 20 μg/mL, and although there was a slight decrease in cell viability, they all exceeded 80%, which indicated good cell viability. This indicates that HA-AZI/Qe-M is safe in cells and is a prerequisite for further experimentation.

Investigating the targets of drug action on MRSA and the targeting of MRSA by drugs has become particularly important.[57–59] The efficacy of drug-loaded micelles for the treatment of intracellular bacterial infections is strongly influenced by cellular uptake.[60,61] Therefore, cellular uptake is a key factor in the micellar drug delivery system. AZI and Qe do not have fluorescent properties, so coumarin was chosen as a fluorescent probe to investigate cellular uptake. Coumarin, a fluorescent probe with a long service life and no cytotoxicity, has been widely used in mechanistic studies of in vivo tracking, cellular uptake, and microparticle drug delivery systems.[62,63] LPS induced RAW264.7 cells were used to simulate the intracellular bacterial infection environment. Flow cytometry and confocal laser microscope were used to quantitatively and qualitatively analyze the uptake of different micelles by RAW264.7 cells. Flow cytometry and CLSM showed that the fluorescence intensity of RAW264.7 cells in HA-Coumarin-M group was the highest. This was due to the activation of CD44 on the surface of macrophages after LPS induction, which promoted the uptake of hyaluronic acid-modified micelles by RAW264.7 cells.

The antibacterial effect in vitro is related to the therapeutic effect of drugs in vivo, and it is also the premise of animal experiments. Inhibition zone, minimum inhibitory concentration, bacterial growth curve and bacterial live/dead staining can be used as indicators to judge the antibacterial effect of drugs. Inhibition zone method is to use the test drug diffusion in LB solid medium to inhibit the growth of bacteria around it to form a circle.[64] It is the most intuitive method to judge the antibacterial effect of drugs according to the size of inhibition circle. In this study, the diameter of inhibition zone of HA-AZI/Qe-M group was 17.48 ± 0.32 mm, indicating that it had a strong inhibitory effect on bacteria (more than 15 mm indicated a strong inhibitory effect).

A lower minimum inhibitory concentration represents a stronger antibacterial potency. The clinical anti-infection treatment is to inhibit the growth of bacteria by rational use of drugs to maintain only the minimum inhibitory concentration, which can avoid excessive drug damage to the body.[65] The minimum inhibitory concentrations of HA-AZI/Qe-M and AZI/Qe-M were 1.25 μg/mL, which was lower than the other groups.

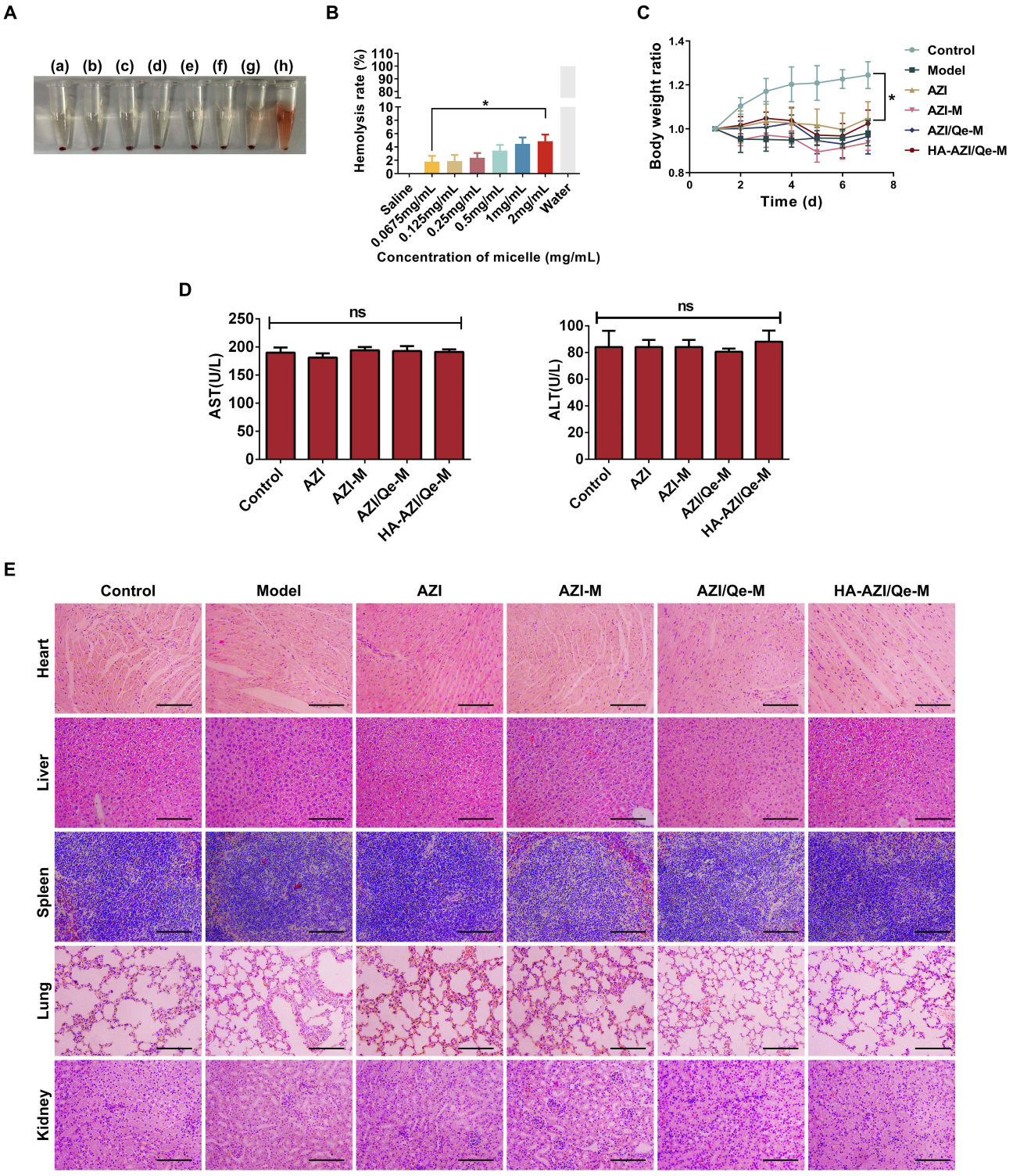

Figure 9 Biocompatibility of HA-AZI/Qe-M. (**A, B**) Hemolysis of HA-AZI/Qe-M (n = 3). (**a**) saline; (**b-g**) HA-AZI/Qe-M concentrations were 0.0675–2mg/mL; (**h**) water. (**C**) Changes in body weight of mice during treatment (n = 6). (**D**) Liver Function Indicators (n = 3). (**E**) HE staining of heart, liver, spleen, lung and kidney of mice one week after intravenous injection of corresponding drugs (n = 6). Scale bar: 50 μm. Control: mice treated with normal saline. Data are presented as mean ± SD (n = 3 or 6). ns = no significance, **P* < 0.05.

Growth curve measurement based on optical density (OD) is one of the most commonly used methods for real-time monitoring of microbial growth and proliferation in microbiology. It provides a simple and reliable method for understanding microorganisms and has been used routinely to determine the growth of bacteria and other microorganisms

treated with antibiotics.[66] We observed that HA-AZI/Qe-M and AZI/Qe-M significantly inhibited MRSA growth, which was superior to the AZI and AZI-M groups.

In the Live/Dead staining assay, SYTO 9 could penetrate the cell membrane of living bacteria and stain the bacteria as green, while propidium iodide (PI) could only penetrate the bacteria with damaged cell membrane and produce red fluorescent cells.[67] Thus bacteria with intact membrane structure appear green and bacteria with damaged membranes appear red. In this experiment, the red fluorescence of HA-AZI/Qe-M and AZI/Qe-M groups was strong, indicating that more bacteria died and the antibacterial effect was good, and the antibacterial effect was stronger than that of AZI and AZI-M groups. In the above experiments, HA-AZI/Qe-M showed excellent antibacterial activity in vitro, which may be due to the addition of the regulator quercetin. However, the antibacterial activity of AZI/Qe-M was almost the same as that of HA-AZI/Qe-M, probably because HA-AZI/Qe-M lacks the ability to target bacteria directly in vitro. We then examined the ability of HA-AZI/Qe-M to treat intracellular bacterial infections.

Intracellular pathogens can cause a variety of diseases, and are an important cause of the increase in the morbidity and mortality of infectious diseases worldwide, which has become an international public health problem.[68] Maintaining intracellular therapeutic concentrations of antibiotics is challenging, and intracellular pathogens are exposed to subtherapeutic concentrations for long periods of time, which is more likely to lead to bacterial resistance to antibiotics.[61] In the intracellular bacteria elimination experiment, HA-AZI/Qe-M group was significantly better than other groups, because HA targeted macrophages and had a significant effect on eliminating intracellular bacteria. We can draw a preliminary conclusion that free AZI reaches the infected cells through passive diffusion, while HA-AZI/Qe-M can enter the cells in large amounts through endocytosis mediated by the highly expressed HA receptor on the macrophage cell membrane, thereby killing intracellular bacteria efficiently.

Bacteria are capable of producing biofilms during growth and reproduction, which cause most chronic and recurrent infections.[69] Biofilm-associated infections recur in approximately 65–80% of cases.[70] Bacteria associated with biofilms are highly resistant to antibiotics.[71] The prevalence of biofilm-mediated infections is very rapid and is observed in periodontitis, endocarditis, osteomyelitis and urinary tract infections.[72] Nanoparticles have been used to overcome biofilms because of their small size, which allows them to easily penetrate into the porous structure of biofilms.[73,74] We hypothesized that micelles with similar properties could also overcome the challenges posed by biofilms. We prepared different micelles and evaluated their biofilm inhibition and removal effects. The MRSA biofilms were incubated with different groups of drugs, and then crystal violet staining and live/dead staining were performed. Both crystal violet staining and live-dead staining showed that HA-AZI/Qe-M and AZI/Qe-M exhibited better biofilm inhibition and clearance than AZI and AZI-M. In conclusion, HA-AZI/Qe-M was able to penetrate deeply into the MRSA biofilm, inhibit and remove the biofilm.

To observe the real-time distribution and retention time of different formulations of micelles in mice, we used a noninvasive optical imaging system to record in vivo fluorescence imaging of mice in real time. The fluorescence of HA-DiR-M reached its peak when it remained at the infection site for 24 hours, and the fluorescence was still present at 96 hours, indicating that the micelles remained in the mice for at least 96 hours. This may be due to the fact that HA-modified micelles can bind to CD44 on the surface of inflammatory macrophages to enter the inflammatory tissue, increase the accumulation of drugs, improve the uptake rate of drugs at the infection site, and achieve the "active targeting" effect.[75] Meanwhile, the surface of micelles was modified with DSPE-PEG_{2000}, and the hydrophobic environment formed by long lipid-acyl chains could accommodate lipophilic drug molecules, thus effectively solubilizing low-water-soluble drugs while restricting the mobility of the incorporated drugs, leading to sustained drug release; the PEG portion of the hydrophilic shell would generate spatial site-blocking, which would stabilize micellar aggregation, reduce the clearance rate of the reticuloendothelial system (RES), and prolong the cycling time of the drug-loaded micelles.[76,77]

Animal models provide opportunities to better study disease progression and pathogenesis and to evaluate potential therapeutic strategies for disease. The tissue was homogenized and plated on LB solid medium, and the number of colonies was counted as a simple and practical method to observe the ability of drugs to clear tissue bacteria. After treatment with HA-AZI/Qe-M, the number of bacteria in thigh muscle tissue of mice was significantly reduced, and it was preliminarily concluded that HA-AZI/Qe-M had excellent antibacterial effect in vivo. Histological analysis is the

basic and main method for biological research and even disease diagnosis. The results of histological analysis show the state of cells and tissues in the organ, allowing us to infer the condition of the whole organism.[78,79] HE staining and Masson staining are commonly used to study the state of cells and tissues. In the results of HE staining, the muscle tissue cells in the blank control group were arranged neatly, the gap was clear, and there was no damage, while the tissue in the model group showed necrosis and inflammatory cell infiltration. After treatment, tissue necrosis was greatly improved and inflammatory cell infiltration was significantly reduced in HA-AZI/Qe-M group. Masson staining collagen levels reflect the level of muscle fibrosis. The collagen deposition in the bacterial infection group was significantly increased, and the collagen deposition in the HA-AZI/Qe-M treatment group was significantly reduced, and the level of collagen deposition was restored to the blank control group. When pathogens invade the body, infection often occurs, which changes the levels of pro-inflammatory factors in the body, leading to immune dysfunction or pathological damage.[80] TNF-α, IL-6 and IL-1β are important pro-inflammatory factors. After bacterial infection, the levels of TNF-α, IL-6 and IL-1β in mice were up-regulated. After treatment with different drugs, HA-AZI/Qe-M could significantly down-regulate the levels of three inflammatory factors in mice, and the levels were similar to those in the blank group, indicating that HA-AZI/Qe-M can significantly inhibit the inflammation caused by bacterial infection. In conclusion, HA-AZI/Qe-M exerts its in vivo antibacterial activity by eliminating bacteria in tissues and relieving inflammation caused by bacterial infection.

The internal environment of animals is quite complex, and nano delivery systems are equivalent to a foreign object, which may cause a series of reactions, such as an immune response to the foreign object, when it enters the organism.[81] In addition, the nanomaterials themselves may also have an effect on the organism.[82] Hemocompatibility evaluation is an important criterion for determining the biosafety of biomaterials, especially those in direct contact with blood.[83] Hemolysis refers to the rupture and dissolution of red blood cells. Because our preparations are injected through the tail vein, some drugs contain hemolytic components or physical or chemical aspects, which will cause hemolysis after injection into the blood vessels. Some drugs can cause blood cell condensation after injection into blood vessels and cause blood circulation disorders, so we need to test the hemolysis of micelles to ensure the biocompatibility of the preparations.[84] The hemolysis rate of the prepared targeted micelles was less than 5%,[85] which indicated that it had good blood compatibility. Due to the presence of long-cycling material DSPE-PEG_{2000}, the residence time of micelles in the body was increased to more than 96h. In addition, after the drug was wrapped in the membrane to form micelles, the toxicity was minimal, which was exactly confirmed by the weight changes and histological examination of mice.

There are several limitations to our study. For example, HA-AZI/Qe-M was constructed to target the macrophages infected with bacteria and showed excellent therapeutic effect against intracellular bacterial infection. However, it did not target bacteria directly, which resulted in less antibacterial effect than those drugs that directly target bacteria in vitro. The antibacterial mechanism of HA-AZI/Qe-M has not been studied, and we will further investigate its antibacterial mechanism in the subsequent experiments.

Conclusion

HA has good biocompatibility, hydrophilicity, biodegradability, non-toxicity, and binding ability to CD44 receptor, making it the best choice for antibacterial and anti-inflammatory drug delivery systems. In this study, we encapsulated AZI and Qe into nano-micelles and modified HA on the surface of the micelles, which greatly improved the drug targeting and therapeutic efficacy against intracellular bacterial infections. The results of cellular uptake assay and anti-intracellular bacterial infection assay showed that HA specifically bound to CD44 on the surface of infected macrophages, significantly enhanced the uptake of micelles by macrophages, thereby achieving targeted clearance of bacteria. HA-AZI/Qe-M has a long circulation time in vivo, accurately targets the infection site, effectively eliminates MRSA at the infection site and reduces muscle tissue damage, and has good biocompatibility. Therefore, we believe that HA-AZI/Qe-M can be used as a promising formulation for the treatment of MRSA infection.

Abbreviations

MRSA, Methicillin-resistant *Staphylococcus aureus*; HA, Hyaluronic acid; Qe, Quercetin; AZI, Azithromycin; HA-AZI/Qe-M, Hyaluronic acid-modified azithromycin and quercetin nano micelles; DSPE-PEG_{2000}, 1,2-Distearoyl-sn-glycero-

3-phosphoethanolamine-N-methoxy-poly (ethylene glycol 2000); $TPGS_{1000}$, D-a-Tocopherol polyethylene glycol 1000 succinate; DiR, 1,1-dioctadecyl-3,3,3,3-tetramethylindotricarbocyanine iodide; FBS, Fetal bovine serum; PBS, Phosphate buffered saline; PDI, Polydispersity index; Blank-M, Blank micelles; AZI-M, Azithromycin micelles; AZI/Qe-M, Azithromycin and quercetin micelles; Coumarin-M, Coumarin micelles; HA-Coumarin-M, Hyaluronic acid-modified coumarin micelles; DiR-M, DiR micelles; HA-DiR-M, Hyaluronic acid-modified DiR micelles; HPLC, High performance liquid phase; TEM, Transmission electron microscope; FTIR, Fourier Transform infrared spectroscopy; ZIP, Zero interaction potentials; SRB, Sulforhodamine B; CLSM, Confocal laser microscope; RBC, Red blood cells; MIC, Minimum inhibitory concentration; HE, Hematoxylin-eosin; TNF-α, Tumor necrosis factor-α; IL-6, Interleukin 6; IL-1β, Interleukin 1β; ALT, Alanine aminotransferase; AST, Aspartate aminotransferase.

Acknowledgments

The Project was supported by the Open fund of Key Laboratory of Ministry of Education for TCM Viscera-State Theory and Applications, Liaoning University of Traditional Chinese Medicine (zyzx2301), China Postdoctoral Science Foundation (2022MD723796), the Doctoral Start-up Foundation of Liaoning Province (2023-BS-139), Basic Research Project of Education Department of Liaoning Province (JYTQN2023471).

Author Contributions

All authors made a significant contribution to the work reported, whether that is in the conception, study design, execution, acquisition of data, analysis and interpretation, or in all these areas; took part in drafting, revising or critically reviewing the article; gave final approval of the version to be published; have agreed on the journal to which the article has been submitted; and agree to be accountable for all aspects of the work. All authors have read and approved the final manuscript.

Disclosure

The authors report no conflicts of interest in this work.

References

1. Beutler B. Innate immune sensing of microbial infection: the mechanism and the therapeutic challenge. *Wien Med Wochenschr*. 2002;152 (21–22):547–551. doi:10.1046/j.1563-258X.2002.02097.x
2. Gould D, Chamberlaine A. Staphylococcus aureus: a review of the literature. *J Clin Nurs*. 1995;4(1):5–12. doi:10.1111/j.1365-2702.1995.tb00004.x
3. Thomer L, Schneewind O, Missiakas D. Pathogenesis of staphylococcus aureus bloodstream infections. *Annu Rev Pathol*. 2016;11(1):343–364. doi:10.1146/annurev-pathol-012615-044351
4. Bruns H, Stenger S. New insights into the interaction of Mycobacterium tuberculosis and human macrophages. *Future Microbiol*. 2014;9 (3):327–341. doi:10.2217/fmb.13.164
5. Soe YM, Bedoui S, Stinear TP, et al. Intracellular Staphylococcus aureus and host cell death pathways. *Cell Microbiol*. 2021;23(5):e13317. doi:10.1111/cmi.13317
6. Ali A, Waris A, Khan MA, et al. Recent advancement, immune responses, and mechanism of action of various vaccines against intracellular bacterial infections. *Life Sci*. 2023;314:121332. doi:10.1016/j.lfs.2022.121332
7. Hommes JW, Surewaard BGJ. Intracellular habitation of staphylococcus aureus: molecular mechanisms and prospects for antimicrobial therapy. *Biomedicines*. 2022;10(8):1804. doi:10.3390/biomedicines10081804
8. Wang Z, Kong L, Liu Y, et al. A phage lysin fused to a cell-penetrating peptide kills intracellular methicillin-resistant staphylococcus aureus in keratinocytes and has potential as a treatment for skin infections in mice. *Appl Environ Microbiol*. 2018a;84(12). doi:10.1128/AEM.00380-18
9. Bhardwaj S, Mehra P, Dhanjal DS, et al. Antibiotics and antibiotic resistance- flipsides of the same coin. *Curr Pharm Des*. 2022;28(28):2312–2329. doi:10.2174/1381612828666220608120238
10. Zinner SH. Antibiotic use: present and future. *New Microbiol*. 2007;30(3):321–325.
11. Akram F, Imtiaz M, Haq IU. Emergent crisis of antibiotic resistance: a silent pandemic threat to 21(st) century. *Microb Pathog*. 2023;174:105923. doi:10.1016/j.micpath.2022.105923
12. Subramaniam G, Girish M. Antibiotic resistance - a cause for reemergence of infections. *Indian J Pediatr*. 2020;87(11):937–944. doi:10.1007/s12098-019-03180-3
13. Porras G, Chassagne F, Lyles JT, et al. Ethnobotany and the role of plant natural products in antibiotic drug discovery. *Chem Rev*. 2021;121 (6):3495–3560. doi:10.1021/acs.chemrev.0c00922
14. Zacchino SA, Butassi E, Liberto MD, et al. Plant phenolics and terpenoids as adjuvants of antibacterial and antifungal drugs. *Phytomedicine*. 2017;37:27–48. doi:10.1016/j.phymed.2017.10.018
15. Cadelis MM, Li SA, van de Pas SJ, et al. Antimicrobial natural products from plant pathogenic fungi. *Molecules*. 2023;28(3):1142. doi:10.3390/molecules28031142

16. Salam AM, Quave CL. Opportunities for plant natural products in infection control. *Curr Opin Microbiol*. 2018;45:189–194. doi:10.1016/j.mib.2018.08.004
17. Firth A, Prathapan P. Azithromycin: the First Broad-spectrum Therapeutic. *Eur J Med Chem*. 2020;207:112739. doi:10.1016/j.ejmech.2020.112739
18. Heidary M, Ebrahimi Samangani A, Kargari A, et al. Mechanism of action, resistance, synergism, and clinical implications of azithromycin. *J Clin Lab Anal*. 2022;36(6):e24427. doi:10.1002/jcla.24427
19. Hsieh HL, Yu M-C, Cheng L-C, et al. Quercetin exerts anti-inflammatory effects via inhibiting tumor necrosis factor-α-induced matrix metalloproteinase-9 expression in normal human gastric epithelial cells. *World J Gastroenterol*. 2022;28(11):1139–1158. doi:10.3748/wjg.v28.i11.1139
20. Kawabata K, Baba N, Sakano T, et al. Functional properties of anti-inflammatory substances from quercetin-treated Bifidobacterium adolescentis. *Biosci Biotechnol Biochem*. 2018;82(4):689–697. doi:10.1080/09168451.2017.1401916
21. Li X, Yang X, Wang Z, et al. Antibacterial, antioxidant and biocompatible nanosized quercetin-PVA xerogel films for wound dressing. *Colloids Surf B Biointerfaces*. 2022;209(Pt 2):112175. doi:10.1016/j.colsurfb.2021.112175
22. Cushnie TP, Lamb AJ. Antimicrobial activity of flavonoids. *Int J Antimicrob Agents*. 2005;26(5):343–356. doi:10.1016/j.ijantimicag.2005.09.002
23. Wang S, Yao J, Zhou B, et al. Bacteriostatic effect of quercetin as an antibiotic alternative in vivo and its antibacterial mechanism in vitro. *J Food Prot*. 2018b;81(1):68–78. doi:10.4315/0362-028X.JFP-17-214
24. Alizadeh SR, Ebrahimzadeh MA. Quercetin derivatives: drug design, development, and biological activities, a review. *Eur J Med Chem*. 2022;229:114068. doi:10.1016/j.ejmech.2021.114068
25. Bi X, Bai Q, Liang M, et al. Silver peroxide nanoparticles for combined antibacterial sonodynamic and photothermal therapy. *Small*. 2022;18(2):e2104160. doi:10.1002/smll.202104160
26. Morena AG, Bassegoda A, Natan M, et al. Antibacterial properties and mechanisms of action of sonoenzymatically synthesized lignin-based nanoparticles. *ACS Appl Mater Interfaces*. 2022;14(33):37270–37279. doi:10.1021/acsami.2c05443
27. Chen X, Yang H, Li C, et al. Enhancing the targeting performance and prolonging the antibacterial effects of clove essential oil liposomes to Campylobacter jejuni by antibody modification. *Food Res Int*. 2023;167:112736. doi:10.1016/j.foodres.2023.112736
28. Emtiazi H, Salari Sharif A, Hemati M, et al. Comparative study of nano-liposome and nano-niosome for delivery of achillea millefolium essential oils: development, optimization, characterization and their cytotoxicity effects on cancer cell lines and antibacterial activity. *Chem Biodivers*. 2022;19(10):e202200397. doi:10.1002/cbdv.202200397
29. Liu Y, Busscher HJ, Zhao B, et al. Surface-adaptive, antimicrobially loaded, micellar nanocarriers with enhanced penetration and killing efficiency in staphylococcal biofilms. *ACS Nano*. 2016;10(4):4779–4789. doi:10.1021/acsnano.6b01370
30. Onat B, Bütün V, Banerjee S, et al. Bacterial anti-adhesive and pH-induced antibacterial agent releasing ultra-thin films of zwitterionic copolymer micelles. *Acta Biomater*. 2016;40:293–309. doi:10.1016/j.actbio.2016.04.033
31. Sousa A, Borøy V, Bæverud A, et al. Polymyxin B stabilized DNA micelles for sustained antibacterial and antibiofilm activity against P. aeruginosa. *J Mater Chem B*. 2023;11(33):7972–7985. doi:10.1039/D3TB00704A
32. Atanase LI. Micellar drug delivery systems based on natural biopolymers. *Polymers*. 2021;13(3):477. doi:10.3390/polym13030477
33. Ghezzi M, Pescina S, Padula C, et al. Polymeric micelles in drug delivery: an insight of the techniques for their characterization and assessment in biorelevant conditions. *J Control Release*. 2021;332:312–336. doi:10.1016/j.jconrel.2021.02.031
34. Patravale VB, Upadhaya PG, Jain RD. Preparation and characterization of micelles. *Methods Mol Biol*. 2019;2000:19–29.
35. Qian J, Guo Y, Xu Y, et al. Combination of micelles and liposomes as a promising drug delivery system: a review. *Drug Deliv Transl Res*. 2023;13(11):2767–2789. doi:10.1007/s13346-023-01368-x
36. Almajidi YQ, Kadhim MM, Alsaikhan F, et al. Doxorubicin-loaded micelles in tumor cell-specific chemotherapy. *Environ Res*. 2023;227:115722. doi:10.1016/j.envres.2023.115722
37. Hazekawa M, Nishinakagawa T, Mori T, et al. Preparation of siRNA-PLGA/Fab'-PLGA mixed micellar system with target cell-specific recognition. *Sci Rep*. 2021;11(1):16789. doi:10.1038/s41598-021-96245-3
38. Zhang X, Wei D, Xu Y, et al. Hyaluronic acid in ocular drug delivery. *Carbohydr Polym*. 2021;264:118006. doi:10.1016/j.carbpol.2021.118006
39. Bukhari SNA, Roswandi NL, Waqas M, et al. Hyaluronic acid, a promising skin rejuvenating biomedicine: a review of recent updates and pre-clinical and clinical investigations on cosmetic and nutricosmetic effects. *Int J Biol Macromol*. 2018;120(Pt B):1682–1695. doi:10.1016/j.ijbiomac.2018.09.188
40. Burdick JA, Prestwich GD. Hyaluronic acid hydrogels for biomedical applications. *Adv Mater*. 2011;23(12):H41–56. doi:10.1002/adma.201003963
41. Huang B, Hu D, Dong A, et al. Highly antibacterial and adhesive hyaluronic acid hydrogel for wound repair. *Biomacromolecules*. 2022;23(11):4766–4777. doi:10.1021/acs.biomac.2c00950
42. Zhou L, Hao Q, Sugita S, et al. Role of CD44 in increasing the potency of mesenchymal stem cell extracellular vesicles by hyaluronic acid in severe pneumonia. *Stem Cell Res Ther*. 2021;12(1):293. doi:10.1186/s13287-021-02329-2
43. Tran TH, Rastogi R, Shelke J, et al. Modulation of macrophage functional polarity towards anti-inflammatory phenotype with plasmid DNA delivery in CD44 targeting hyaluronic acid nanoparticles. *Sci Rep*. 2015;5(1):16632. doi:10.1038/srep16632
44. Fu Q, Wei Z, Xiao P, et al. CD44 enhances macrophage phagocytosis and plays a protective role in Streptococcus equi subsp. zooepidemicus infection. *Vet Microbiol*. 2017;198:121–126. doi:10.1016/j.vetmic.2016.12.030
45. Mod R, Chan SY, Widodo RT, et al. Optimization of a luteolin-loaded TPGS/Poloxamer 407 nanomicelle: the effects of copolymers, hydration temperature and duration, and freezing temperature on encapsulation efficiency, particle size, and solubility. *Cancers*. 2023;15(14):3741. doi:10.3390/cancers15143741
46. Zhang Q, Zhou Y, Feng X, et al. Low-dose orlistat promotes the therapeutic effect of oxaliplatin in colorectal cancer. *Biomed Pharmacother*. 2022;153:113426. doi:10.1016/j.biopha.2022.113426
47. El G, Eldera SS, Kenawy SH, et al. Hydroxyapatite nanoparticles derived from mussel shells for in vitro cytotoxicity test and cell viability. *Heliyon*. 2020;6(6):e04085. doi:10.1016/j.heliyon.2020.e04085
48. Guo RB, Zhang X-Y, Yan D-K, et al. Folate-modified triptolide liposomes target activated macrophages for safe rheumatoid arthritis therapy. *Biomater Sci*. 2022;10(2):499–513. doi:10.1039/D1BM01520F
49. Shi C, Zhang Z, Shi J, et al. Co-delivery of docetaxel and chloroquine via PEO-PPO-PCL/TPGS micelles for overcoming multidrug resistance. *Int J Pharm*. 2015;495(2):932–939. doi:10.1016/j.ijpharm.2015.10.009

50. Duan Y, He K, Zhang G, et al. Photoresponsive micelles enabling codelivery of nitric oxide and formaldehyde for combinatorial antibacterial applications. *Biomacromolecules*. 2021;22(5):2160–2170. doi:10.1021/acs.biomac.1c00251
51. Grossman AB, Burgin DJ, Rice KC. Quantification of staphylococcus aureus biofilm formation by crystal violet and confocal microscopy. *Methods Mol Biol*. 2021;2341:69–78.
52. Che J, Okeke C, Hu Z-B, et al. DSPE-PEG: a distinctive component in drug delivery system. *Curr Pharm Des*. 2015;21(12):1598–1605. doi:10.2174/1381612821666150115144003
53. Xiong Q, Cui M, Bai Y, et al. A supramolecular nanoparticle system based on β-cyclodextrin-conjugated poly-l-lysine and hyaluronic acid for co-delivery of gene and chemotherapy agent targeting hepatocellular carcinoma. *Colloids Surf B Biointerfaces*. 2017;155:93–103. doi:10.1016/j.colsurfb.2017.04.008
54. Verma AK, Kumar A. Pharmacokinetics and biodistribution of negatively charged pectin nanoparticles encapsulating paclitaxel. *Cancer Nanotechnol*. 2013;4(4–5):99–102. doi:10.1007/s12645-013-0041-8
55. Rizeq BR, Younes NN, Rasool K, et al. Synthesis, bioapplications, and toxicity evaluation of chitosan-based nanoparticles. *Int J Mol Sci*. 2019;20(22):5776. doi:10.3390/ijms20225776
56. Sun S, Zhang J, Li H, et al. Anti-inflammatory activity of the water extract of chloranthus serratus roots in LPS-stimulated RAW264.7 cells mediated by the Nrf2/HO-1, MAPK and NF-κB signaling pathways. *J Ethnopharmacol*. 2021;271:113880. doi:10.1016/j.jep.2021.113880
57. Dalal V, Dhankhar P, Singh V, et al. Structure-based identification of potential drugs against FmtA of staphylococcus aureus: virtual screening, molecular dynamics, MM-GBSA, and QM/MM. *Protein J*. 2021;40(2):148–165. doi:10.1007/s10930-020-09953-6
58. Kumari R, Dalal V, et al. Identification of potential inhibitors for LLM of Staphylococcus aureus: structure-based pharmacophore modeling, molecular dynamics, and binding free energy studies. *J Biomol Struct Dyn*. 2022;40(20):9833–9847. doi:10.1080/07391102.2021.1936179
59. Dhankhar P, et al. I*n-silico approach to identify novel potent inhibitors against GraR of S. aureus*. *Front Biosci*. 2020;25(7):1337–1360. doi:10.2741/4859
60. Adjei IM, Sharma B, Labhasetwar V. Nanoparticles: cellular uptake and cytotoxicity. *Adv Exp Med Biol*. 2014;811:73–91.
61. Li J, Cheng X, Chen Y, et al. Vitamin E TPGS modified liposomes enhance cellular uptake and targeted delivery of luteolin: an in vivo/in vitro evaluation. *Int J Pharm*. 2016;512(1):262–272. doi:10.1016/j.ijpharm.2016.08.037
62. Dou T, Wang J, Han C, et al. Cellular uptake and transport characteristics of chitosan modified nanoparticles in Caco-2 cell monolayers. *Int J Biol Macromol*. 2019;138:791–799. doi:10.1016/j.ijbiomac.2019.07.168
63. Xue L, Yu D, Sun J, et al. Rapid GSH detection and versatile peptide/protein labelling to track cell penetration using coumarin-based probes. *Analyst*. 2023;148(3):532–538. doi:10.1039/D2AN01510B
64. Shi H, Zhuang Q, Zheng A, et al. Antibacterial mechanism of N-PMI and the characteristics of PMMA-Co-N-PMI copolymer. *Chem Biodivers*. 2022;19(6):e202100753. doi:10.1002/cbdv.202100753
65. Lowman W. Minimum inhibitory concentration-guided antimicrobial therapy - the achilles heel in the antimicrobial stewardship agenda. *S Afr Med J*. 2018;108(9):710–712. doi:10.7196/SAMJ.2018.v108i9.13285
66. Krishnamurthi VR, Niyonshuti II, Chen J, et al. A new analysis method for evaluating bacterial growth with microplate readers. *PLoS One*. 2021;16(1):e0245205. doi:10.1371/journal.pone.0245205
67. Tawakoli PN, Al-Ahmad A, Hoth-Hannig W, et al. Comparison of different live/dead stainings for detection and quantification of adherent microorganisms in the initial oral biofilm. *Clin Oral Investig*. 2013;17(3):841–850. doi:10.1007/s00784-012-0792-3
68. Jiao J, Wang J, Fu J. Editorial: new advances in obligate intracellular bacteria: pathogenesis and host interactions. *Front Cell Infect Microbiol*. 2023;13:1338697. doi:10.3389/fcimb.2023.1338697
69. Rabin N, Zheng Y, Opoku-Temeng C, et al. Biofilm formation mechanisms and targets for developing antibiofilm agents. *Future Med Chem*. 2015;7(4):493–512. doi:10.4155/fmc.15.6
70. Del Pozo JL. Biofilm-related disease. *Expert Rev Anti Infect Ther*. 2018;16(1):51–65. doi:10.1080/14787210.2018.1417036
71. Venkatesan N, Perumal G, Doble M. Bacterial resistance in biofilm-associated bacteria. *Future Microbiol*. 2015;10(11):1743–1750. doi:10.2217/fmb.15.69
72. Mirzaei R, Mohammadzadeh R, Alikhani MY, et al. The biofilm-associated bacterial infections unrelated to indwelling devices. *IUBMB Life*. 2020;72(7):1271–1285. doi:10.1002/iub.2266
73. AlMatar M, Makky EA, Var I, et al. The role of nanoparticles in the inhibition of multidrug-resistant bacteria and biofilms. *Curr Drug Deliv*. 2018;15(4):470–484. doi:10.2174/1567201815666171207163504
74. Gallo G, Schillaci D. Bacterial metal nanoparticles to develop new weapons against bacterial biofilms and infections. *Appl Microbiol Biotechnol*. 2021;105(13):5357–5366. doi:10.1007/s00253-021-11418-4
75. Salathia S, Gigliobianco MR, Casadidio C, et al. Hyaluronic acid-based nanosystems for cd44 mediated anti-inflammatory and antinociceptive activity. *Int J Mol Sci*. 2023;24(8):7286. doi:10.3390/ijms24087286
76. Alexis F, Pridgen E, Molnar LK, et al. Factors affecting the clearance and biodistribution of polymeric nanoparticles. *Mol Pharm*. 2008;5(4):505–515. doi:10.1021/mp800051m
77. Maeda H, Wu J, Sawa T, et al. Tumor vascular permeability and the EPR effect in macromolecular therapeutics: a review. *J Control Release*. 2000;65(1–2):271–284. doi:10.1016/S0168-3659(99)00248-5
78. de Haan K, Zhang Y, Zuckerman JE, et al. Deep learning-based transformation of H&E stained tissues into special stains. *Nat Commun*. 2021;12(1):4884. doi:10.1038/s41467-021-25221-2
79. Tandon A, Singh A, Shetty D, et al. Tetrachromic VOF/Masson's trichrome/H and E stains: unmasking their usability in differential stromal hard tissue staining. *Indian J Pathol Microbiol*. 2019;62(1):67–72. doi:10.4103/IJPM.IJPM_242_18
80. Jiao Y, Sun J, Bacterial manipulation of autophagic responses in infection and inflammation. *Front Immunol*, 2019. 10: p. 2821.
81. Gao C, Huang Q, Liu C, et al. Treatment of atherosclerosis by macrophage-biomimetic nanoparticles via targeted pharmacotherapy and sequestration of proinflammatory cytokines. *Nat Commun*. 2020;11(1):2622. doi:10.1038/s41467-020-16439-7
82. Ali A, Ovais M, Cui X, et al. Safety assessment of nanomaterials for antimicrobial applications. *Chem Res Toxicol*. 2020;33(5):1082–1109. doi:10.1021/acs.chemrestox.9b00519
83. Feyerabend F, Wendel H-P, Mihailova B, et al. Blood compatibility of magnesium and its alloys. *Acta Biomater*. 2015;25:384–394. doi:10.1016/j.actbio.2015.07.029

84. Chen L, Han D, Jiang L, et al. On improving blood compatibility: from bioinspired to synthetic design and fabrication of biointerfacial topography at micro/nano scales. *Colloids Surf B Biointerfaces*. 2011;85(1):2–7. doi:10.1016/j.colsurfb.2010.10.034
85. Li T, Wang P, Guo W, et al. Natural berberine-based chinese herb medicine assembled nanostructures with modified antibacterial application. *ACS Nano*. 2019;13(6):6770–6781. doi:10.1021/acsnano.9b01346